

Anisotropic Iron Motion in Nitrosyl Iron Porphyrinates: Natural and Synthetic Hemes

Jeffrey W. Pavlik,^{†,¶} Qian Peng,^{†,¶} Nathan J. Silvernail,[†] E. Ercan Alp,[‡] Michael Y. Hu,[‡] Jiyong Zhao,[‡] J. Timothy Sage,^{*,§} and W. Robert Scheidt^{*,†}

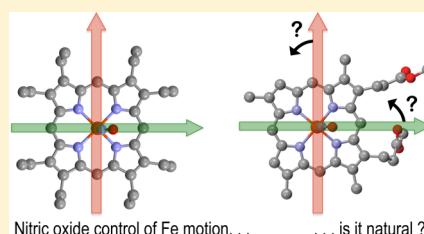
[†]Department of Chemistry and Biochemistry, University of Notre Dame, Notre Dame, Indiana 46556, United States

[‡]Advanced Photon Source, Argonne National Laboratory, Argonne, Illinois 60439, United States

[§]Department of Physics and Center for Interdisciplinary Research on Complex Systems, Northeastern University, 120 Forsyth Street, Boston, Massachusetts 02115, United States

S Supporting Information

ABSTRACT: The vibrational spectra of two five-coordinate nitrosyl iron porphyrinates, [Fe(OEP)(NO)] (OEP = dianion of 2,3,7,8,12,13,17,18-octaethylporphyrin) and [Fe(DPIX)(NO)] (DPIX = deuteroporphyrin IX), have been studied by oriented single-crystal nuclear resonance vibrational spectroscopy. Single crystals (both are in the triclinic crystal system) were oriented to give vibrational spectra perpendicular to the porphyrin plane. Additionally, two orthogonal in-plane measurements that were also either perpendicular or parallel to the projection of the FeNO plane onto the porphyrin plane yield the complete set of vibrations with iron motion. In addition to cleanly enabling the assignment of the FeNO bending and stretching modes, the measurements reveal that the two in-plane spectra from the parallel and perpendicular in-plane directions for both compounds have substantial differences. The assignment of these in-plane vibrations were aided by density functional theory predictions. The differences in the two in-plane directions result from the strongly bonded axial NO ligand. The direction of the in-plane iron motion is thus found to be largely parallel and perpendicular to the projection of the FeNO plane on the porphyrin plane. These axial ligand effects on the in-plane iron motion are related to the strength of the axial ligand-to-iron bond.



INTRODUCTION

Nitric oxide (NO) was once thought to be just a toxic gas but is now recognized as an essential biological signaling agent and was *Science's* molecule of the year in 1992.¹ As is now well-known, NO is important in blood-pressure regulation, as a neurotransmitter, as well as a (toxic) defense mechanism in neutrophils and macrophages.^{2–13} NO is synthesized by a family of heme enzymes that catalyze the 7-electron oxidation of L-arginine to NO.^{14–20}

Vibrational spectroscopy has long been used as a structural probe for nitrosyl iron porphyrinates. In biological signaling processes, heme proteins discriminate between NO, CO, and O₂ quite efficiently in a number of systems.^{21–24} This selectivity is not always explained by weak-force interactions between the diatomic molecule and the binding pocket, and phenomena intrinsic to the heme prosthetic group may be partly responsible. Vibrational frequencies can be used to illuminate coordination-site and ligand bonding subtleties beyond that discernible by X-ray crystallography alone.²⁵

Nuclear resonance vibrational spectroscopy (NRVS) is a relatively new addition to the vibrational toolbox that allows for a more robust vibrational evaluation of heme complexes in the low-frequency region of the spectrum. NRVS detects the displacement of iron (or other Mössbauer active nuclides) along the direction of the incident beam, and thus peak intensity measured from single crystals is dependent upon

sample orientation.^{26–36} For porphyrin crystals with all porphyrin planes mutually parallel, spectra have been typically collected in two orientations, one with the porphyrin planes normal to the incident beam for observation of modes with out-of-plane (oop or z-direction) iron motion and a second with the porphyrin planes parallel to the beam for observation of modes with in-plane (ip) iron motion. In the original oop/ip experiments, the in-plane direction was arbitrarily selected and taken to represent a generalized in-plane spectrum.

Recently, a specialized in-plane (SIP) NRVS method was developed in which spectra are taken at two in-plane directions perpendicular to each other.³⁷ One direction is in-plane and also parallel to a feature of chemical significance in the complex (in-plane-*x*) and the other is in-plane and also normal to the first (in-plane-*y*). The three spectra (oop, in-plane-*x*, and in-plane-*y*) taken along three mutually perpendicular directions together ensure the observation of intensity from all modes with iron displacement and together reveal the spatial trajectory of the iron center within each mode.

[Fe(OEP)(NO)]³⁸ (OEP = dianion of 2,3,7,8,12,13,17,18-octaethylporphyrin) was selected for the initial SIP experiment because its NO ligand is well-ordered and because suitable crystals are more easily obtained, compared to other [Fe-

Received: November 21, 2013

Published: February 14, 2014

(Porph)(NO)] (Porph = dianion of generalized porphyrin) complexes. Nitrosyl iron porphyrinates often exhibit disorder of the NO group over two or more axial positions, an apparent consequence of the well-documented low barrier to rotation about the Fe–N_{NO} bond.^{39–41} In this initial experiment, strong in-plane anisotropy in [Fe(OEP)(NO)] was observed, and the vibrational modes had distinctly different in-plane-*x* and in-plane-*y* components.³⁷ The in-plane-*x* measurement was parallel to the Fe–N–O projection onto the porphyrin mean plane, while that of in-plane-*y* was normal to this direction.

An understanding of the in-plane anisotropy was aided by a density functional theory (DFT) spectral prediction using the BP86 functional and a TZVP basis set. In the calculation, the predicted frequencies and mode intensities were in good agreement, although with some differences between the observed and predicted spectra. The detailed information available from this experiment led us to explore DFT predictions from several different functionals.⁴² The SIP NRVS method provides a unique opportunity to evaluate DFT calculations because the directional (*x*, *y*, and *z*) displacements of iron (and all other atoms) within all vibrational modes are provided in the DFT output files. From these values, directionally specific predicted spectra (predicted vibrational density of states or VDOS) are generated for each direction and are designated as $D_x(\bar{\nu})$, $D_y(\bar{\nu})$ and $D_z(\bar{\nu})$. The DFT calculations can therefore be evaluated not only for accuracy of predicted frequency but also for iron directionality, which may help to differentiate between the influences of the ligand versus porphyrin peripheral groups on iron motion. These results demonstrated that the calculations based on the M06-L functional with a TZVP basis set for iron was even better than that given by the BP86 calculation, and the details of the M06-L prediction will first be discussed in this paper.

We continued these detailed in-plane measurements with a related species [Fe(DPIX)(NO)] (DPIX = deuteroporphyrin IX). We were especially concerned with the question of potential influences of asymmetric peripheral substituents. DPIX is closely related to protoporphyrin IX (i.e., the dianion of protoporphyrin IX dimethyl ester (PPIX)) employed by nature in many heme proteins, and that would have been preferred for this study. Unfortunately, the PPIX derivative was found to have a disordered NO and large thermal parameters for the porphyrin ring.⁴⁴ It was therefore unsuitable for this experiment. Therefore, the deuteroporphyrin-IX dimethylester derivative was employed. An earlier crystal structure determination⁴⁵ had shown that [Fe(DPIX)(NO)] was completely suitable for the experiment. We report the NRVS spectra obtained in three orientations including the two in-plane measurements with the probing X-ray beam parallel and perpendicular to the projection of the FeNO group onto the porphyrin plane. We used DFT predictions to aid in the detailed assignment of the in-plane spectra. We find that in both species the NO ligand has strong effects on the iron in-plane direction that are described herein.

EXPERIMENTAL SECTION

General Information. All reactions and manipulations for the preparation of the iron(II) porphyrin derivatives were carried out under argon using a double manifold vacuum line, Schlenkware, and cannula techniques. Dichloromethane, toluene, and hexanes were distilled under argon over CaH₂ and sodium/benzophenone. Chlorobenzene was purified by washing with concentrated sulfuric acid, then with water until the aqueous layer was neutral, dried with

sodium sulfate, and distilled twice over P₂O₅. 95% ⁵⁷Fe₂O₃ was purchased from Cambridge Isotopes. H₂OEP was synthesized by literature methods.⁴⁶ Nitric oxide (Mittler Specialty Gases) was purified by fractional distillation through a trap containing 4 Å molecular sieves bathed in a dry ice/ethanol slurry.⁴⁷

Small-Scale Metalation. Insertion of ⁵⁷Fe into free-base porphyrins was conducted in purified chlorobenzene according to a modified Landergrén method as follows.⁴⁸ Approximately 2 mL of 12 M HCl was used to dissolve ~0.20 mmol 95% ⁵⁷Fe enriched Fe₂O₃ contained in a 250 mL Schlenk flask. After 5 min of stirring, the HCl was removed under vacuum to near dryness, and subsequent steps of the metalation reaction were done in an inert environment using standard Schlenk procedures. Failure to maintain an inert environment will likely result in an incomplete or inefficient metal insertion. Freshly distilled chlorobenzene (100 mL) was added via cannula, and the mixture was refluxed for 2 h in a hot oil bath. Half of the chlorobenzene was removed by distillation, and 10 mL of a chlorobenzene solution containing ~0.15 mmol of H₂Porph and 0.4 mL of 2,4,6-collidine was added via cannula. After refluxing for 3 h, chlorobenzene was removed under vacuum, and the residue was dissolved in 50 mL of CH₂Cl₂. The solution was washed twice with 50 mL of DI water, thrice with 50 mL of 1 M HCl, and once with 50 mL of DI water. After drying over Na₂SO₄ and filtering through a sintered-glass filter, solvent was removed by rotoevaporation. Minimal CH₂Cl₂ was used to redissolve the product and transfer to an evaporation dish. The remaining solvent was evaporated using very low heat.

Reductive Nitrosylation. Chloroporphyrinatoiron(III) compounds were reductively nitrosylated under argon, and all solvents used were degassed by sparging with argon for 5 min. Liquid–liquid diffusion crystallization was done with methanol as the counter solvent in 40 cm × 7 mm glass tubes sealed with rubber septa. Crystals were typically harvested after about 10 d, washed with methanol, and immediately mounted for the NRVS orientation procedure.

[⁵⁷Fe(OEP)(NO)]. After metalation as described above, the resulting [⁵⁷Fe(OEP)(Cl)] was reductively nitrosylated: 75 mg (0.12 mmol) was dissolved in 2.5 mL of CHCl₃, 0.2 mL of pyridine, and 0.2 mL of methanol then sparged with nitric oxide for 5 min. The reaction solution was divided between four glass tubes for crystallization by liquid–liquid diffusion.

[⁵⁷Fe(DPIX)(NO)]. Free-base deuteroporphyrin IX dimethyl ester was purchased from Frontier Scientific. After metalation as described above, the resulting [⁵⁷Fe(DPIX)(Cl)] was reductively nitrosylated: 30 mg (0.05 mmol) was dissolved in 1.5 mL of CHCl₃, 0.1 mL of pyridine, and 0.1 mL of methanol then sparged with nitric oxide for 5 min. The reaction solution was divided between three glass tubes for crystallization by liquid–liquid diffusion.

Crystal Mounting. Crystals were mounted onto specially prepared dual arc goniometer heads. Copper wire, 4–5 cm in length and 18 gauge, was affixed to the goniometer and bent into a u-shape. A glass fiber, 5–8 mm in length, was then superglued to project along the goniometer ϕ -axis. The connection of the wire into the goniometer head was fortified with epoxy resin. A crystal was then affixed to the tip of the glass fiber using super glue. The wire was then carefully bent so that the crystal was approximately on the ϕ -axis and then stretched to the required height for centering. Crystals were then oriented for NRVS analysis along specified in-plane axes by methods described in the Supporting Information.

NRVS Spectra. Spectra were measured at Sector 3-ID at the Advanced Photon Source, Argonne National Laboratory, Argonne IL. Powders were milled with a minimal amount of Apiezon-M vacuum grease, then put into the 1 × 2 × 10 mm³ cavity of a 3 × 8 × 15 mm³ polystyrene sample “coffin”, which was directly mounted in a He flow cryostat, and cooled to 20 K. Single-crystal samples were previously mounted and aligned on goniometer heads that were now screwed into place on a rotating stage. The mounted crystals were then navigated into the X-ray beam by translations of the stage and rotated to the predetermined ϕ angle required for the particular direction of analysis desired. Vibration spectra were measured using an in-line high-resolution monochromator operating at 14.4125 keV with 1.0 meV bandwidth scanning the energy of incident X-ray beam.⁴⁹ Spectra

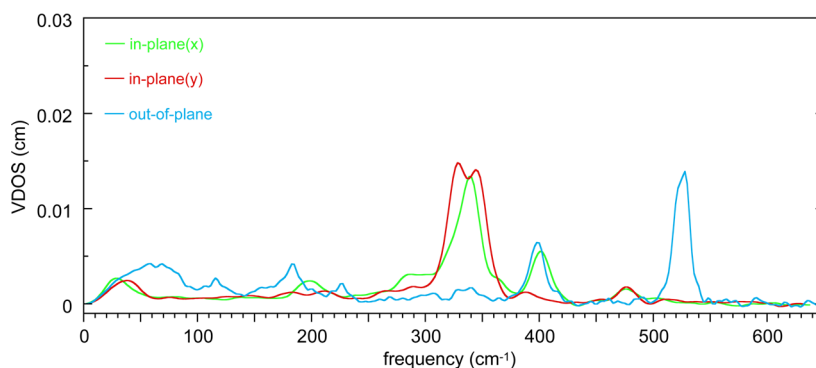


Figure 1. Directional contributions to the VDOS of [Fe(DPIX)(NO)]. (blue) Out-of-plane. (green) In-plane-*x*. (red) In-plane-*y*.

were recorded between -30 and 80 meV in steps of 0.25 meV, and all scans (3–6 replicates) were normalized to the intensity of the incident beam and added. NRVs raw data were converted to the VDOS using the program PHOENIX.^{26,50}

For both NO species, measurements were made with three directions of the analyzing X-ray beam, either normal to the porphyrin plane (the *z* direction) or parallel to the porphyrin plane and also either perpendicular (the *y*-direction) or parallel (the *x*-direction) to the FeNO plane.

Vibrational Predictions and Predicted Mode Composition Factors e^2 . The Gaussian09 program package⁵¹ was used to optimize the structures and for frequency analysis. The $S = 1/2$ complexes [Fe(OEP)(NO)] and [Fe(DPIX)(NO)] were fully optimized without any constraints, using the spin-unrestricted DFT method. The starting structure was obtained from the crystal structure of triclinic [Fe(OEP)(NO)]^{52,53} and [Fe(DPIX)(NO)].⁴⁵ Frequency calculations were performed on the fully optimized structures at the same level to obtain the vibrational frequencies of the ⁵⁷Fe isotope set. The frequencies reported here were not scaled. The frequency data were created using the high-precision format vibrational frequency eigenvectors to calculate mode composition factors (e^2) and VDOS as described below.

We studied two classes of functionals: (1) generalized gradient approximation (GGA) functionals (BP86),⁵⁴ which contain the exchange and GGA correlation functionals, and (2) meta-GGA functional (M06-L),⁵⁵ which is a local meta-GGA functional. In general, we used triple- ζ valence basis sets with polarization functions (TZVP)⁵⁶ on iron and 6-31G* for all other atoms.

The G09 output files from the DFT calculations can be used to generate predicted mode composition factors with our scripts.⁴² The mode composition factors $e_{j\alpha}^2$ for atom *j* and frequency mode α are the fraction of total kinetic energy contributed by atom *j* (here: ⁵⁷Fe, the NRVs active nucleus). The normal mode calculations are obtained from the atomic displacement matrix together with the equation

$$(e_{j\alpha, \text{inplane}})^2 = \frac{m_j(r_{jx}^2 + r_{jy}^2)}{\sum m_i r_i^2} \quad (1)$$

where the sum over *i* runs over all atoms of the molecule, m_i is the atomic mass of atom *i*, and r_i is the absolute length of the Cartesian displacement vector for atom *i*. The polarized mode composition factors are defined in terms of two distinct in-plane directions, which can be calculated from a projection of the atomic displacement vectors *x* and *y* (eq 1).⁵⁸ The out-of-plane atomic displacement perpendicular to the resulting porphyrin plane for a normal mode is obtained from a projection of the atomic displacement vector *z* (eq 2).

$$(e_{j\alpha, \text{outofplane}})^2 = \frac{m_j r_{jz}^2}{\sum m_i r_i^2} \quad (2)$$

The *x*, *y*, and *z* components of the iron normal mode energy for [Fe(OEP)(NO)] and [Fe(DPIX)(NO)] with $e_{\text{Fe}}^2 \geq 0.005$ are given in Tables S2–S5 of the Supporting Information.

The predicted mode composition factors $e_{j\alpha}^2$ can also be compared to the integrated spectral areas obtained from NRVs. Therefore VDOS intensities can be simulated from the mode composition factors, using the Gaussian normal distributions function, where the full width at half height (fwhh) is defined appropriately by considering the spectral resolution in the experiment. In this study, the MATLAB R2010a software was used to generate the predicted NRVs curves.

RESULTS

The directionally dependent NRVs spectra in the three orthogonal directions are shown for [Fe(OEP)(NO)]³⁷ in Supporting Information, Figure S1 and for [Fe(DPIX)(NO)] in Figure 1. The dominant in-plane NRVs region occurs between 250 and 425 cm^{-1} for both [Fe(OEP)(NO)] and [Fe(DPIX)(NO)]. For [Fe(OEP)(NO)] this region includes peaks of moderate intensity at ~ 310 cm^{-1} , the strongest in-plane peaks, 350 cm^{-1} for in-plane-*x* and 342 cm^{-1} for in-plane-*y*, and the Fe–N–O bending mode that only shows in-plane signal in the *x*-direction. For [Fe(DPIX)(NO)] the central, most intense peaks are 342 cm^{-1} for in-plane-*x* and 331 and 347 cm^{-1} for in-plane-*y* (Figure 1, green and red lines). The peaks to the lower-frequency side of the strongest peaks are of significantly lower intensity than the corresponding peaks in [Fe(OEP)(NO)] and the bending mode at 401 cm^{-1} for [Fe(DPIX)(NO)] that has an in-plane-*x* but no in-plane-*y* signal.

The out-of-plane NRVs spectra each exhibit vibrations involving porphyrin distortions in addition to a doming mode, the *z*-component of the Fe–N–O bend, and the Fe–N_{NO} stretching mode. For [Fe(OEP)(NO)] and [Fe(DPIX)(NO)], respectively, porphyrin doming contributes to modes at 158 and 183 cm^{-1} , Fe–N–O bending contributes to modes at 394 and 399 cm^{-1} , and Fe–N_{NO} stretching contributes to modes at 517 and 528 cm^{-1} . Vibrational correlation analysis⁵⁷ indicates that doming contributes to additional out-of-plane signal(s) in the very low-frequency range (<100 cm^{-1}) observable (Figure 1, blue) above the lattice vibrational modes, which can be seen as broad peaks between 0 and 80 cm^{-1} in the in-plane spectra (Figure 1, green and red). DFT calculations for predictions of the vibrational spectra for both complexes were carried out utilizing two different functionals (BP86 and M06-L). Comparisons of the experimental spectra and theoretical predictions will be discussed subsequently.

Spectral Predictions. The results of DFT calculations are shown in figures cited throughout the paper. Figures include experimental NRVs (line traces) overlaid on the corresponding predicted NRVs spectra (shaded) and predicted mode composition factors or $e_{\text{Fe}_n}^2$ (bars) for $n = x, y, z$. Figure 2

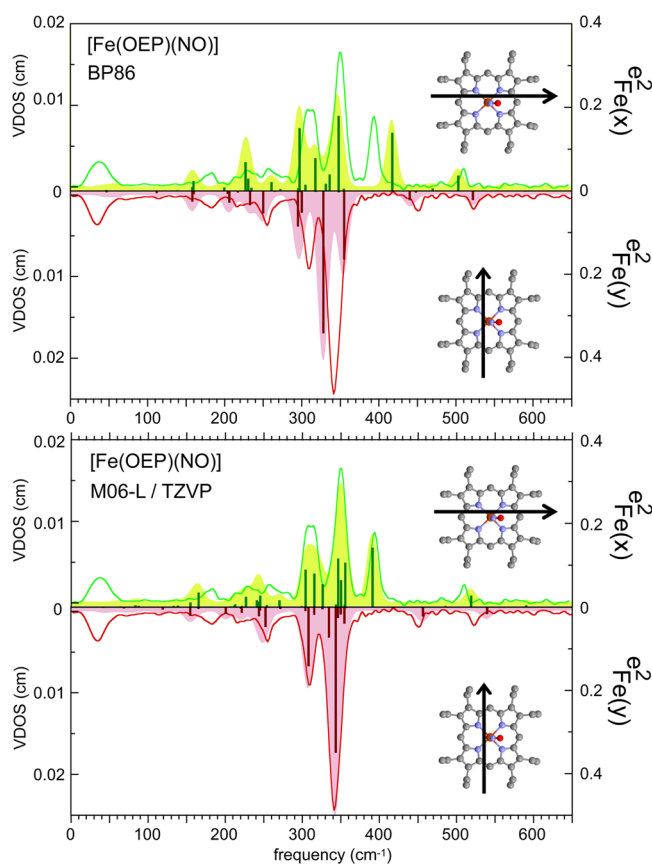


Figure 2. In-plane “mirror” plots of $[\text{Fe}(\text{OEP})(\text{NO})]$ that display the (line) measured and (shaded) predicted contributions to the VDOS from Fe motion. (green traces) Observed in-plane- x . (light green, shaded spectra) Predicted D_x . (dark green bars) Predicted $e_{\text{Fe}_x}^2$. (red line) Observed in-plane- y . (pink, shaded spectra) Predicted D_y . (dark red bars) Predicted $e_{\text{Fe}_y}^2$. Direction of the X-ray beam indicated by the black arrow. Predictions made using (top) BP86/TZVP and (bottom) M06-L/TZVP.

shows the in-plane predictions for $[\text{Fe}(\text{OEP})(\text{NO})]$ from the BP86 and M06-L functionals, which shows the significantly higher quality predictions from the M06-L calculation. Supporting Information, Figure S2 shows the out-of-plane predictions for $[\text{Fe}(\text{OEP})(\text{NO})]$ from the BP86 and M06-L functionals. Figure 3 shows the in-plane predictions for $[\text{Fe}(\text{DPIX})(\text{NO})]$ from the BP86 and M06-L functionals. Figure 4 shows the out-of-plane predictions for $[\text{Fe}(\text{DPIX})(\text{NO})]$ from the BP86 and M06-L functionals. The in-plane- y spectra in Figures 2 and 3 are shown with the ordinate axes inverted to facilitate in-plane- x versus in-plane- y frequency comparisons. An initial assessment of DFT accuracy can be assessed visually from the figures by comparing the predicted and experimental VDOS.

DISCUSSION

In an earlier communication,³⁷ we had explored the vibrational spectrum of the nitrosyl complex $[\text{Fe}(\text{OEP})(\text{NO})]$ with specially oriented crystal specimens. In this Paper we are again concerned with specially oriented crystals for a related species, $[\text{Fe}(\text{DPIX})(\text{NO})]$, with asymmetrical peripheral substituents. The $[\text{Fe}(\text{OEP})(\text{NO})]$ study demonstrated that the anisotropy of in-plane vibrations could be resolved by appropriate oriented single-crystal measurements. The combi-

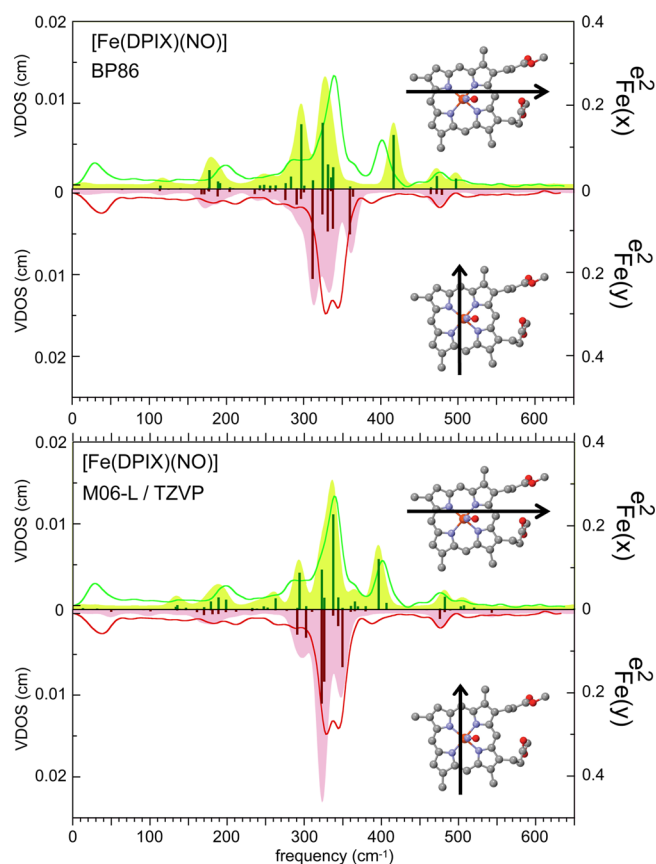


Figure 3. In-plane “mirror” plots of $[\text{Fe}(\text{DPIX})(\text{NO})]$ that display the (line) measured and (shaded) predicted contributions to the VDOS from Fe atom motion. (green trace) Observed in-plane- x . (light green, shaded spectra) Predicted D_x . (dark green bars) Predicted $e_{\text{Fe}_x}^2$. (red line) Observed in-plane- y . (pink, shaded spectra) Predicted D_y . (dark red bars) Predicted $e_{\text{Fe}_y}^2$. Direction of the X-ray beam indicated by the black arrow. Predictions made using (top) BP86/TZVP and (bottom) M06-L/TZVP.

nation of the experimental spectra and DFT vibrational predictions showed that the in-plane vibrational modes were highly influenced by the nitrosyl ligand; the iron motion was predominantly either along or normal to the Fe–N–O plane. Thus the orientation of the axial NO ligand, rather than the direction of the in-plane iron–porphyrin nitrogen (Fe–N_p) bonds, controls the direction of the in-plane iron motion.

We expanded upon that study with an analysis of a DFT calculation based on the functional M06-L/TZVP for $[\text{Fe}(\text{OEP})(\text{NO})]$, which had clearly proven to be the most accurate VDOS predictor, as established by an in-depth comparison of a multitude of functional/basis set combinations.⁴² The M06-L-based calculation is shown to be superior in both mode frequency accuracy and iron motion directionality relative to the earlier BP86 calculation.

The top portion of Figure 2 shows the experimental in-plane vibrational spectrum and the results of the DFT predictions based on a BP86 functional calculation; the two orthogonal in-plane directions are shown. As had been discussed previously,³⁷ this combination of experiment and calculations allowed us to reach the conclusion that the orientation of the bent FeNO group controlled the direction of the in-plane iron motion. We now show that predictions based on the use of the M06-L functional⁵⁵ provide even better agreement in the prominent

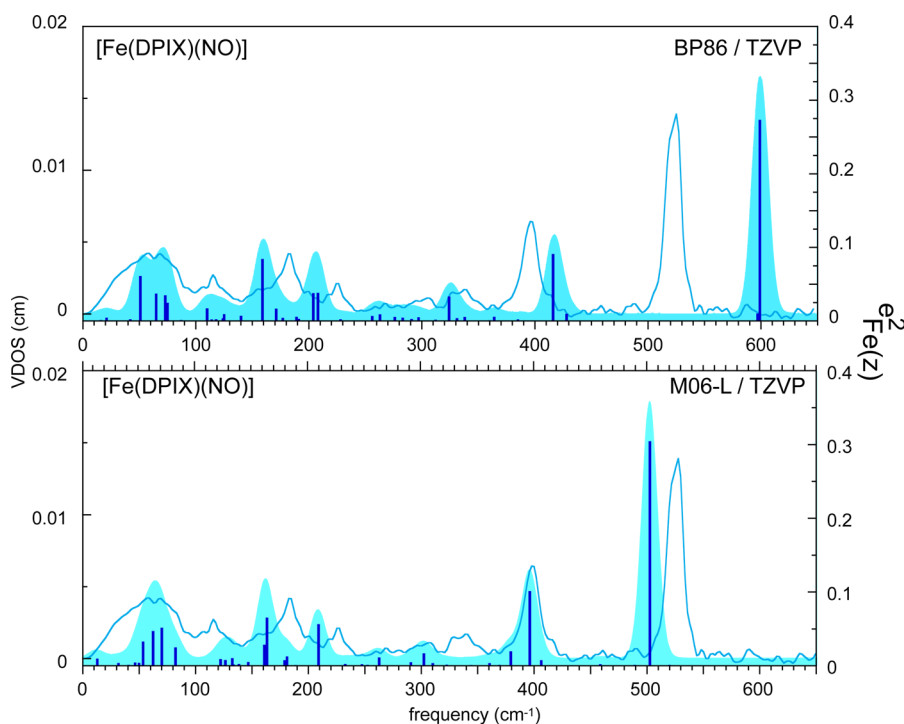


Figure 4. Out-of-plane contributions to the VDOS from Fe atom motion for (blue traces) [Fe(DPIX)(NO)], (light blue shaded, top) BP86/TZVP predicted VDOS, (light blue shaded, bottom) M06-L/TZVP predicted VDOS, and (dark blue bars) $e_{\text{Fe}_z}^2$.

in-plane region between 280 and 370 cm^{-1} , as can be seen in the bottom portion of Figure 2. For the peaks at $\sim 300 \text{ cm}^{-1}$ of in-plane- x , the BP86/TZVP prediction gives two peaks, one apparently underestimated in frequency and the other in intensity, whereas M06-L/TZVP appears to have the mode frequencies well-predicted and lacks only slightly in predicted intensity. In-plane- y at $\sim 300 \text{ cm}^{-1}$ is underestimated in frequency by BP86/TZVP and nearly perfectly predicted by M06-L/TZVP. The remainder of the prominent in-plane peaks are predicted exceedingly well by M06-L/TZVP, even in peak shape, consistent with an accurate prediction of the smaller satellites of the 343 cm^{-1} mode of in-plane- y and the trio of moderate-intensity modes that contribute to the 350 cm^{-1} observed peak in in-plane- x .

In the lower-frequency region, below 280 cm^{-1} , the M06-L/TZVP-predicted VDOS are marginally better than those of BP86/TZVP, owing mostly to the overpredicted peak intensities, ~ 210 in-plane- y and $\sim 230 \text{ cm}^{-1}$ in-plane- x of the latter. The nearly identical peaks at 182 and 183 cm^{-1} that appear in both the x - and y -experimental spectra have predicted frequencies low by $\sim 20 \text{ cm}^{-1}$, and the BP86/TZVP calculation comes closer to forecasting their observed degeneracy. The weak peaks in the higher-frequency regime above 370 cm^{-1} are predicted slightly better in frequency by BP86/TZVP, but the same calculation severely overestimates the Fe–N–O bending mode frequency: 394 cm^{-1} observed and 417 cm^{-1} predicted.

The improvement in agreement between experiment and prediction extends to the out-of-plane portion of the spectrum as well, as can be seen in Supporting Information, Figure S2 that shows the out-of-plane component. M06-L/TZVP perfectly predicts the Fe–N–O bending mode frequency and $e_{\text{Fe}_z}^2$. As can be seen in Supporting Information, Figure S2, $e_{\text{Fe}_z}^2$ is moderately underestimated by the same calculation. Also apparent in Supporting Information, Figure S2 is the overestimation of Fe–NO stretching frequency by BP86/

TZVP: 623 cm^{-1} predicted and 517 cm^{-1} observed. M06-L/TZVP predicts this mode at 477 cm^{-1} , a significant improvement. Other peaks of interest are the iron-doming mode observed at 158 cm^{-1} and the very low-frequency modes, below 100 cm^{-1} , all of which have predicted frequencies underestimated by 10–20 cm^{-1} by both calculations. The very low frequency modes have significant observed intensity above the lattice modes, only in the out-of-plane or z -direction, as demonstrated in Supporting Information, Figure S1 (blue trace, 50–100 cm^{-1}).

Supporting Information, Figures S3 and S4 show the predicted x , y , and z components of all modes with significant iron contributions from the BP86 and M06-L predictions, respectively. As noted, both calculations display very good agreement with the experimental data. The two bar graphs clearly show that the directional character of all major in-plane modes are predominantly either x or y . In this definition of the coordinate system, x is in the plane defined by the projection of the FeNO plane, and y is perpendicular to the FeNO plane. As expected, with this coordinate frame, the bending mode has only x and z components. We conclude that the orientation of the bent axial FeNO group, and not the direction of the in-plane Fe–N_p bonds, controls the direction of all major in-plane iron motion.

What features of the [Fe(OEP)(NO)] molecule lead to such strongly polarized vibrational spectra? The vibrational spectra appear to reflect the strong asymmetry in the interaction between the Fe d_π orbitals and the NO π^* orbitals parallel and perpendicular to the FeNO plane, owing to the nonlinear Fe–N–O group and the extra (odd) electron in the NO π^* orbital. As we have noted recently,⁵⁹ this effect is clearly related to the strength of the axial Fe–X bond with ligands that remove the 4-fold degeneracy. For a series of [Fe(OEP)(X)] species, the control of iron directionality is NO > general imidazolate (Im[−]) > general imidazole (HIm).

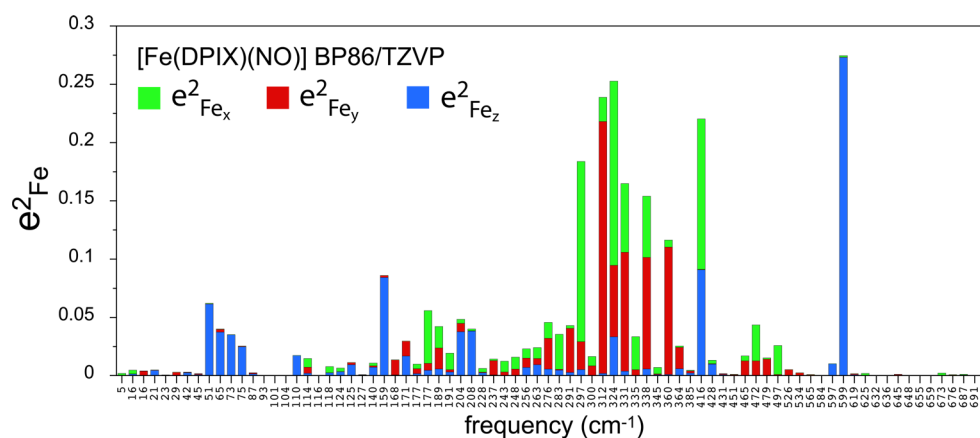


Figure 5. Mode composition factors of $[\text{Fe}(\text{DPIX})(\text{NO})]$. Total column height represents iron kinetic energy fraction for modes. Height of colored segments reflects the directional components of the iron kinetic energy fraction. (green) $e_{\text{Fe}_x}^2$. (red) $e_{\text{Fe}_y}^2$. (blue) $e_{\text{Fe}_z}^2$. Predictions made using BP86/TZVP.

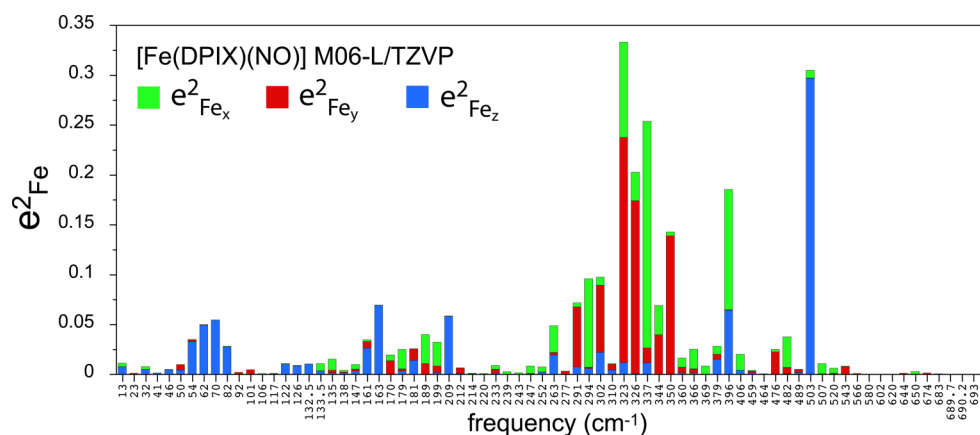


Figure 6. Mode composition factors of $[\text{Fe}(\text{DPIX})(\text{NO})]$. Total column height represents iron kinetic energy fraction for modes. Height of colored segments reflects the directional components of the iron kinetic energy fraction. (green) $e_{\text{Fe}_x}^2$. (red) $e_{\text{Fe}_y}^2$. (blue) $e_{\text{Fe}_z}^2$. Predictions made using M06-L/TZVP.

We have now extended the detailed oriented crystal NRVS measurements and calculations to a “natural” nitrosyl porphyrin derivative. The oriented single-crystal measurements require that the molecules crystallize in a system where all porphyrin planes are parallel to each other and that the axial ligands be ordered and have the same relative orientation. These requirements are met by $[\text{Fe}(\text{DPIX})(\text{NO})]$,⁴⁵ but not by $[\text{Fe}(\text{PIX})(\text{NO})]$. Unfortunately, $[\text{Fe}(\text{PIX})(\text{NO})]$, which was finally crystallized after much effort, has a disordered NO group.⁴⁴

Detailed oriented single-crystal NRVS spectra and DFT calculations were also obtained for “natural” $[\text{Fe}(\text{DPIX})(\text{NO})]$, that is, a derivative with a peripheral substituent pattern similar to that of protoporphyrin IX.⁶⁰ Figure 3 shows the experimental in-plane vibrational spectra in two orthogonal directions and the results of the DFT predictions based on the BP86 functional calculation (top); the spectral results based on the M06-L predictions are shown in the bottom panel. Figure 4 provides the information obtained for the oriented crystal data in the out-of-plane (heme normal) direction. Satisfactory predictions of the out-of-plane vibrations have always been the more difficult challenge for DFT calculations,³⁴ but Figure 4 clearly shows that the M06-L-based predictions are satisfying and superior. Both peak frequencies and intensities are in good

agreement, especially the Fe–NO stretching frequency predicted at 503 cm^{-1} and observed at 528 cm^{-1} . The FeNO bending frequency is observed at 399 cm^{-1} and predicted at 396 cm^{-1} .

The M06-L predictions are also seen to be superior for the in-plane spectra (Figure 3). The intense in-plane bands between 250 and 400 cm^{-1} are predicted by the M06-L calculation in both the x and y directions to within a few wavenumbers. The intensity of the shoulders around 290 cm^{-1} in both directions are moderately overestimated but agree well in frequency. The central in-plane- x mode at 297 cm^{-1} is predicted strikingly well, as are the shoulder at 365 cm^{-1} and the bending mode at 401 cm^{-1} . The greatest discrepancy is in the intensity proportioning of the double peak observed at 329 and 345 cm^{-1} in the in-plane- y spectrum. However, if the 337 cm^{-1} peak (one of the two predicted modes at 323 and 337 cm^{-1}) would be shifted to higher frequency by only $\sim 10\text{ cm}^{-1}$, the double peak intensities would become more even.

Figures 5 and 6 display bar graphs showing the directional character of the iron motion in $[\text{Fe}(\text{DPIX})(\text{NO})]$ from two DFT predictions. The predictions for M06-L (Figure 6), which we believe to be the more reliable, show that the in-plane iron motion is mostly in directions that are either parallel or perpendicular to the FeNO plane and not along the Fe– N_p

directions. Thus the orientation of the axial Fe–N–O group is most important for the in-plane vibrational directions. This is similar to what has been concluded for the [Fe(OEP)(NO)] case. This can be seen in the predicted character of the six most intense in-plane vibrations for [Fe(DPIX)(NO)] shown in the MOLEKEL⁶¹ depictions of Figure 7. The Fe–N–O orientation

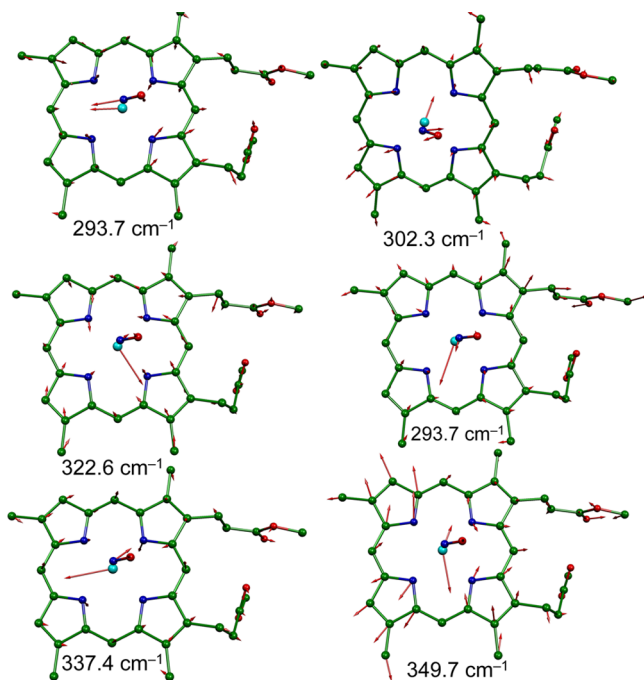


Figure 7. MOLEKEL depictions of the six most intense ($e_{\text{Fe}}^2 > 0.096$) in-plane vibrations based on the M06-L predictions.

effects may be slightly modified by the asymmetric effects of peripheral substituents. Previous powder measurements on Fe(Porph)(NO)], where derivatives included DPIX, PPIX, and the dianion of mesoporphyrin IX dimethyl ester (MPIX), showed that small changes in the peripheral porphyrin substituents had real effects on the iron in-plane vibrational envelope.⁶²

Although the differences in the structures between [Fe(OEP)(NO)]⁵³ and [Fe(DPIX)(NO)]⁴⁵ are marginally significant, at best, the differences are consistent with the observed differences in the vibrational data. The length of the Fe–N(NO) bond is 1.7307(7) Å in the OEP derivative and 1.723(3) Å in the DPIX derivative, consistent with the lower-frequency value of 517 cm⁻¹ in OEP and the 528 cm⁻¹ value in DPIX. The doming mode differences (158 cm⁻¹ in OEP and 183 cm⁻¹ in DPIX) might correlate with the small differences in displacement from the four nitrogen-atom plane (0.28 Å in OEP and 0.26 Å in DPIX), although vibrational mixing with out-of-plane substituent displacement may also contribute. Predicting the structural effects on the FeNO bend appears to be more difficult, and in any case, there is not a meaningful difference in the two Fe–N–O angles (142.7(1)° in OEP and 143.1(3)° in DPIX).

The current studies continue to demonstrate the unusual properties of NO as a ligand in iron porphyrinate systems, especially those of {FeNO}⁷ systems. These include a strong trans-directing influence in six-coordinate {FeNO}⁷ species,^{32–36,63,64} the off-axis tilting of the Fe–NO bond in both five- and six-coordinate {FeNO}⁷ complexes,^{52,53,65} along with

the induced asymmetry of the equatorial Fe–N_p bonds, and the importance of the FeNO orientation on the direction of in-plane iron motion.^{37,42} The present investigation extends these conclusions to a β -substituted porphyrin system more closely resembling biologically occurring hemes. Although the biological significance of the structural deviations from axial symmetry remain to be explored, the observation of five-coordinate nitrosyl hemes in NO-signaling proteins^{66,67} continues to fuel discussion of the contribution of the trans-directing influence of NO to activation of these proteins.

The important effects of the NO orientation on the iron vibrational spectrum appears to continue to be significant in related six-coordinate species. SIP NRVS data collection and analysis on a crystallographically appropriate six-coordinate NO derivative are in progress.

Summary. Detailed experimental and theoretical analyses of oriented single-crystal NRVS of two five-coordinate NO derivatives, [Fe(OEP)(NO)] and [Fe(DPIX)(NO)], show that the strongly bonded axial NO ligand markedly affects the direction of the in-plane iron motion. The major directions of the in-plane motion are parallel and perpendicular to the projection of the FeNO plane onto the porphyrin plane. These directions are oblique to the direction of the in-plane Fe–N_p bonds. The effects of the axial ligand on the in-plane iron motion appears to be related to the strength of the axial bonding.

■ ASSOCIATED CONTENT

📄 Supporting Information

A description of the crystal orientation process for the out-of-plane and SIP-in-plane measurements. Figures S1–S4, giving previously published information on the NRVS spectra of [Fe(OEP)(NO)]. Tables giving e_{Fe}^2 values >0.01 for [Fe(OEP)(NO)], Fe(DPIX)(NO)], Fe(MPIX)(NO)], and [Fe(MPIX)(NO)], including complete directional values. This material is available free of charge via the Internet at <http://pubs.acs.org>.

■ AUTHOR INFORMATION

✉ Corresponding Author

*E-mail: jtsage@neu.edu (J.T.S.), scheidt.1@nd.edu (W.R.S.).

👤 Author Contributions

¶These workers contributed equally to this work.

📝 Notes

The authors declare no competing financial interest.

■ ACKNOWLEDGMENTS

We thank the National Institutes of Health for support of this research under Grant GM-38401 to W.R.S. and the National Science Foundation under CHE-1026369 to J.T.S. Use of the Advanced Photon Source, an Office of Science User Facility operated for the U.S. Department of Energy (DOE) Office of Science by Argonne National Laboratory, was supported by the U.S. DOE under Contract No. DE-AC02-06CH11357. We thank Dr. Allen G. Oliver for assistance with crystal alignments.

■ REFERENCES

- (1) Culotta, E.; Koshland, D. E. *Science* **1992**, *258*, 1862.
- (2) Kots, A. Y.; Martin, E.; Sharina, I. G.; Murad, F. In *Handbook of Experimental Pharmacology*; Schmidt, H. H.; Hofmann, F.; Stasch, J.-P., Eds.; Springer-Verlag: Berlin, 2009; pp 1–14.
- (3) Russwurm, M.; Koesling, D. *EMBO J.* **2004**, *23*, 4443.

- (4) Moncada, S.; Palmer, R. M. J.; Higgs, E. A. *Pharmacol. Rev.* **1991**, *43*, 109.
- (5) Snyder, S. H. *Science* **1992**, *257*, 494.
- (6) Butler, A. R.; Williams, D. L. H. *Chem. Soc. Rev.* **1993**, 233.
- (7) Stamler, J. S.; Singel, D. J.; Loscalzo, J. *Science* **1992**, *258*, 1898.
- (8) Hughes, M. N. *Biochim. Biophys. Acta* **1999**, *1411*, 263.
- (9) Walker, F. A. *J. Inorg. Biochem.* **2005**, *99*, 216.
- (10) Cooper, C. E. *Biochim. Biophys. Acta* **1999**, *1411*, 290.
- (11) Drapier, J.-C.; Pellat, C.; Henry, Y. *J. Biol. Chem.* **1991**, *266*, 10162.
- (12) Stadler, J.; Bergonia, H. A.; Di Silvio, M.; Sweetland, M. A.; Billiar, T. R.; Simmons, R. L.; Lancaster, J. R. *Arch. Biochem. Biophys.* **1993**, *302*, 4.
- (13) Terenzi, F.; Diaz-Guerra, M. J. M.; Casado, M.; Hortelano, S.; Leoni, S.; Bosca, L. *J. Biol. Chem.* **1995**, *270*, 6017.
- (14) Griffith, W.; Stuehr, D. *J. Annu. Rev. Physiol.* **1995**, *57*, 707.
- (15) Wang, J.; Stuehr, D. J.; Ikeda-Saito, M.; Rousseau, D. L. *J. Biol. Chem.* **1993**, *268*, 22255.
- (16) Crane, B. R.; Arvai, A. S.; Ghosh, D. K.; Wu, C.; Getzoff, E. D.; Stuehr, D. J.; Tainer, J. A. *Science* **1998**, *279*, 2121.
- (17) Li, H.; Poulos, T. L. *J. Inorg. Biochem.* **2005**, *99*, 293.
- (18) Marletta, M. A. *J. Biol. Chem.* **1993**, *268*, 12231.
- (19) Rousseau, D. L.; Li, D.; Couture, M.; Yeh, S.-R. *J. Inorg. Biochem.* **2005**, *99*, 306.
- (20) Bredt, D. S.; Snyder, S. H. *Annu. Rev. Biochem.* **1994**, *63*, 175.
- (21) Rodgers, K. R. *Curr. Opin. Chem. Biol.* **1999**, *3*, 158.
- (22) Ma, X.; Sayed, N.; Bueve, A.; van den Akker, F. *EMBO J.* **2007**, *26*, 578.
- (23) Nioche, P.; Berka, V.; Vipond, J.; Minton, N.; Tsai, A.; Raman, C. S. *Science* **2004**, *306*, 1550.
- (24) Erbil, W. K.; Price, M. S.; Wemmer, D. E.; Marletta, M. A. *Proc. Natl. Acad. Sci. U.S.A.* **2009**, *106*, 19753.
- (25) Zhu, L.; Sage, J. T.; Champion, P. M. *Science* **1994**, *266*, 629.
- (26) Sage, J. T.; Paxson, C.; Wyllie, G. R. A.; Sturhahn, W.; Durbin, S. M.; Champion, P. M.; Alp, E. E.; Scheidt, W. R. *J. Phys. Condens. Matter.* **2001**, *13*, 7707.
- (27) Scheidt, W. R.; Durbin, S. M.; Sage, J. T. *J. Inorg. Biochem.* **2005**, *99*, 60.
- (28) Sturhahn, W. *J. Phys. Condens. Matter.* **2006**, *16*, S497.
- (29) Kohn, V. G.; Chumakov, A. I.; Rüffer, R. *Phys. Rev. B: Condens. Matter Mater. Phys.* **1998**, *58*, 8437.
- (30) Parlinski, K.; Łażewski, J.; Jochym, P. T.; Chumakov, A. I.; Rüffer, R.; Kresse, G. *Europhys. Lett.* **2001**, *56*, 275.
- (31) Petrenko, T.; Sturhahn, W.; Neese, F. *Hyperfine Interact.* **2007**, *175*, 165.
- (32) Li, J.-F.; Peng, Q.; Barabanchikov, A.; Pavlik, J. W.; Alp, E. E.; Sturhahn, W.; Zhao, J.; Schulz, C. E.; Sage, J. T.; Scheidt, W. R. *Chem.—Eur. J.* **2011**, *17*, 11178.
- (33) Li, J.-F.; Peng, Q.; Barabanchikov, A.; Pavlik, J. W.; Alp, E. E.; Sturhahn, W.; Zhao, J.; Sage, J. T.; Scheidt, W. R. *Inorg. Chem.* **2012**, *51*, 11769.
- (34) Zeng, W.; Silvernail, N. J.; Wharton, D. C.; Georgiev, G. Y.; Leu, B. M.; Scheidt, W. R.; Zhao, J.; Sturhahn, W.; Alp, E. E.; Sage, J. T. *J. Am. Chem. Soc.* **2005**, *127*, 11200.
- (35) Silvernail, N. J.; Barabanchikov, A.; Pavlik, J. W.; Noll, B. C.; Zhao, J.; Alp, E. E.; Sturhahn, W.; Sage, J. T.; Scheidt, W. R. *J. Am. Chem. Soc.* **2007**, *129*, 2200.
- (36) Lehnert, N.; Sage, J. T.; Silvernail, N. J.; Scheidt, W. R.; Alp, E. E.; Sturhahn, W.; Zhao, J. *Inorg. Chem.* **2010**, *49*, 7197.
- (37) Pavlik, J. W.; Barabanchikov, A.; Oliver, A. G.; Alp, E. E.; Sturhahn, W.; Zhao, J.; Sage, J. T.; Scheidt, W. R. *Angew. Chem., Int. Ed. Engl.* **2010**, *49*, 4400.
- (38) The following abbreviations are used in this paper: OEP, dianion of 2,3,7,8,12,13,17,18-octaethylporphyrin; DPIX, dianion of deuteroporphyrin IX dimethyl ester; PPIX, dianion of protoporphyrin IX dimethyl ester; MPIX, dianion of mesoporphyrin IX dimethyl ester; Porph, dianion of generalized porphyrin; Im⁻, general imidazolate; HIm, general imidazole; VDOS, vibrational density of states; NRVs, nuclear resonance vibrational spectroscopy.
- (39) Patchkovskii, S.; Ziegler, T. *Inorg. Chem.* **2000**, *39*, 5354.
- (40) Silvernail, N. J.; Pavlik, J. W.; Noll, B. C.; Schulz, C. E.; Scheidt, W. R. *Inorg. Chem.* **2008**, *47*, 912.
- (41) Silvernail, N. J.; Barabanchikov, A.; Sage, J. T.; Noll, B. C.; Scheidt, W. R. *J. Am. Chem. Soc.* **2009**, *131*, 2131.
- (42) Peng, Q.; Pavlik, J. W.; Scheidt, W. R.; Wiest, O. *J. Chem. Theory Comput.* **2012**, *8*, 214 This paper explored eight different functionals with varying basis sets and tabulated comparisons of experimental and predicted structural and vibrational data. Other comparisons had been previously done in Reference 43.
- (43) Lehnert, N.; Galinato, M. G. I.; Paulat, F.; Richter-Addo, G. B.; Sturhahn, W.; Xu, N.; Zhao, J. *Inorg. Chem.* **2010**, *49*, 4133 This paper explored the use of B3LYP and BP86 with varying basis sets.
- (44) Wyllie, G. R. A.; Silvernail, N. J.; Oliver, A. G.; Scheidt, W. R., manuscript in preparation.
- (45) Wyllie, G. R. A.; Scheidt, W. R. *Inorg. Chem.* **2003**, *42*, 4259.
- (46) Milgram, B. C.; Eskildsen, K.; Richter, S. M.; Scheidt, W. R.; Scheidt, K. A. *J. Org. Chem.* **2007**, *72*, 3941.
- (47) Dodd, R. E.; Robinson, P. L. *Experimental Inorganic Chemistry*; Elsevier: New York, 1957; p 253.
- (48) Landergrén, M.; Baltzer, L. *Inorg. Chem.* **1990**, *29*, 556.
- (49) Toellner, T. S. *Hyperfine Interact.* **2000**, *125*, 3.
- (50) Sturhahn, W.; Toellner, T. S.; Alp, E. E.; Zhang, X. W.; Ando, M.; Yoda, Y.; Kikuta, S.; Seto, M.; Kimball, C. W.; Dabrowski, B. *Phys. Rev. Lett.* **1995**, *74*, 3832.
- (51) Frisch, M. J.; Trucks, G. W.; Schlegel, H. B.; Scuseria, G. E.; Robb, M. A.; Cheeseman, J. R.; Scalmani, G.; Barone, V.; Mennucci, B.; Petersson, G. A.; Nakatsuji, H.; Caricato, M.; Li, X.; Hratchian, H. P.; Izmaylov, A. F.; Bloino, J.; Zheng, G.; Sonnenberg, J. L.; Hada, M.; Ehara, M.; Toyota, K.; Fukuda, R.; Hasegawa, J.; Ishida, M.; Nakajima, T.; Honda, Y.; Kitao, O.; Nakai, H.; Vreven, T.; Montgomery, J. A., Jr.; Peralta, J. E.; Ogliaro, F.; Bearpark, M.; Heyd, J. J.; Brothers, E.; Kudin, K. N.; Staroverov, V. N.; Kobayashi, R.; Normand, J.; Raghavachari, K.; Rendell, A.; Burant, J. C.; Iyengar, S. S.; Tomasi, J.; Cossi, M.; Rega, N.; Millam, J. M.; Klene, M.; Knox, J. E.; Cross, J. B.; Bakken, V.; Adamo, C.; Jaramillo, J.; Gomperts, R.; Stratmann, R. E.; Yazyev, O.; Austin, A. J.; Cammi, R.; Pomelli, C.; Ochterski, J. W.; Martin, R. L.; Morokuma, K.; Zakrzewski, V. G.; Voth, G. A.; Salvador, P.; Dannenberg, J. J.; Dapprich, S.; Daniels, A. D.; Farkas, O.; Foresman, J. B.; Ortiz, J. V.; Cioslowski, J.; Fox, D. J.; *Gaussian 09*, Revision A.02; Gaussian, Inc.: Wallingford, CT, 2009.
- (52) Ellison, M. K.; Scheidt, W. R. *J. Am. Chem. Soc.* **1997**, *119*, 7404.
- (53) Scheidt, W. R.; Duval, H. F.; Neal, T. J.; Ellison, M. K. *J. Am. Chem. Soc.* **2000**, *122*, 4651.
- (54) (a) Becke, A. D. *Phys. Rev.* **1988**, *A38*, 3098. (b) Perdew, J. P. *Phys. Rev. B: Condens. Matter Mater. Phys.* **1986**, *33*, 8822.
- (55) Zhao, Y.; Truhlar, D. G. *J. Chem. Phys.* **2006**, *125*, 194101.
- (56) Schäfer, A.; Horn, H.; Ahlrichs, R. *J. Chem. Phys.* **1992**, *97*, 2571.
- (57) Barabanchikov, A.; Demidov, A.; Kubo, M.; Champion, P. M.; Sage, J. T.; Zhao, J.; Sturhahn, W.; Alp, E. E. *J. Chem. Phys.* **2011**, *135*, 015101.
- (58) The definitions of the *x* and *y* in this paper has *x* parallel to the Fe–N–O plane and *y* perpendicular to the Fe–N–O plane.
- (59) Peng, Q.; Li, M.; Hu, C.; Pavlik, J. W.; Oliver, A. G.; Alp, E. E.; Hu, M. Y.; Zhao, J.; Sage, J. T.; Scheidt, W. R. *Inorg. Chem.* **2013**, *52*, 11361.
- (60) The 2,4-vinyl groups in protoporphyrin IX are replaced with hydrogen atoms in deuteroporphyrin IX.
- (61) Portmann, S.; Lüthi, H. P. *Chimia* **2000**, *54*, 766.
- (62) Leu, B.; Zgierski, M.; Wyllie, G. R. A.; Scheidt, W. R.; Sturhahn, W.; Alp, E. E.; Durbin, S. M.; Sage, J. T. *J. Am. Chem. Soc.* **2004**, *126*, 4211.
- (63) Scheidt, W. R.; Piciulo, P. L. *J. Am. Chem. Soc.* **1976**, *98*, 1913.
- (64) Traylor, T. G.; Sharma. *Biochemistry* **1992**, *31*, 2847.
- (65) Wyllie, G. R. A.; Schulz, C. E.; Scheidt, W. R. *Inorg. Chem.* **2003**, *42*, 5722–5734.
- (66) Denninger, J. W.; Marletta, M. A. *Biochim. Biophys. Acta* **1999**, *1441*, 334.

(67) Andrew, C. R.; George, S. J.; Lawson, D. M.; Eady, R. R.
Biochemistry **2002**, *41*, 2353.